Metasurface-Enabled Tri-Band Coplanar Decagon Antenna Design and Analysis for Next-Generation Vehicular Communication

Akansha Gupta [1], Purnima K. Sharma [2], T. J. V. Subrahmanyeswara Rao [3,*], T. V. N. L. Aswini [4], and Dinesh Sharma [5]

[1] Department of Electrical and Computer Engineering, Graphic Era University, Dehradun, India
[2] Institute of Engineering and Technology, Chitkara University, Punjab 140401, India
[3] Department of Electrical and Computer Engineering, Sasi Institute of Technology and Engineering, Tadepalligudem, AP, India
[4] Department of Electrical and Computer Engineering, Sri Vasavi Engineering College, Tadepalligudem, AP, India
[5] Department of Electrical and Computer Engineering, Chandigarh College of Engineering and Technology, Chandigarh, India
Email: akanshagupta.cse@geu.ac.in (A.G.); Purnima.kadali@gmail.com (P.K.S.); tjvsrao@gmail.com (T.J.V.S.R.); aswini.thota@srivasaviengg.ac.in (T.V.N.L.A); dsharma@ccet.ac.in (D.S.)

***Abstract*—This work aims to design a tri-band coplanar decagon-shaped antenna suited for vehicular communication using a metasurface approach. In order to serve applications including Global Positioning System (GPS), Long Term Evolution (LTE), Wi-Fi, and vehicular communication, this research paper develops a coplanar decagon-shaped antenna with dimensions of 30 mm × 30 mm × 1.6 mm. A decagon-shaped Split Ring Resonator (SRR) that is coplanar oriented with respect to the ground is incorporated into the antenna design. The emission pattern of the radio waves radiated by the driven element is manipulated by strategically implementing two L-shaped slots and four parasitic elements. By directing the waves in a specific beam, this modification enhances the antenna's directivity (gain). Interestingly, the addition of metamaterial to the suggested design improved the efficiency from 60% to 87%, affecting the antenna's gain and other radiative characteristics. The performance investigation demonstrates that the proposed antenna attains a gain of 3.2 dBi, 1.13 dBi, 4.6 dBi across multiple operating bands. The HFSS software is used to run the simulation in its entirety.**

***Keywords*—metamaterial, split ring resonator, parasitic elements, left-handed material**

I. Introduction

Recently, growing attention has been directed to vehicular communication systems because of their potential to improve surface traffic safety and efficiency. The general idea is that future cars will gather sensor data and use wireless connectivity to communicate with the road infrastructure and other cars about traffic dynamics. The kind of vehicle seeking communication and the location of antennas on the vehicle are two important "environmental factors" affecting these systems. As it regulates the multipath components that can reach the antenna, the cumulative effect of these parameters not only determines the communication influence of the subject car but also impacts how much other blocking automobiles influence the channel.

Presently, the majority of antennas put on cars are located on the roof or next to the back window; extra antennas, mostly for radar purposes, are located in the bumper and sometimes even on the dashboard. It is interesting to note that there have not been many Vehicles to Vehicle (V2V) measuring experiments carried out using antennas in business cars that are actively in use [1]. The radiation properties of an antenna are sometimes altered by the presence of obstacles, which makes an analysis of the antenna's impact on a massive metal body necessary.

Vehicle communication antennas are mounted on Printed Circuit Board (PCB) circuits or neatly tucked into the shark fin on the roof of the automobile, giving drivers a variety of placement possibilities inside the vehicle [2−4]. As an alternative, particular spots for antenna installation have been chosen, taking into consideration the antenna's characteristics while on the car, such as the roof, side mirrors, bumpers, windows, and trunk. The use of fractal geometries [5], stubs [6], different slot shapes [7], and numerous rings [8] are some of the methods that have been proposed to enable multiband operations in small antennas. It is possible to achieve band notching qualities by using Split Ring Resonator (SRR) slots, adding stubs, and carefully placing slots in the radiating structure.

The decagon structure of the antenna naturally accommodates compatibility with Meta surface Patterns. the placement of concentric SRRs with split gaps, facilitating both the desired magnetic dipole response and the spatial distribution [9].

A magnetic response is produced by the SRR's interruptions, and capacitance is introduced by the gap in

Manuscript received June 30, 2025; revised September 10, 2025; accepted October 16, 2025; published February 25, 2026.

the SRR. Crucially, every ring in the SRR plays a part in producing a unique resonant frequency [10]. Table I compares various existing antenna designs for Vehicular Communication (V2X).

TABLE I. COMPARISON OF EXISTING ANTENNA DESIGN FOR V2X

Ref.	Shape of patch antenna	Dimensions	Substrate	Resonant Frequencies	Gain
[6]	Triple band notch compact MIMO antenna with defected ground structure and split ring resonator	24 × 28 × 1 mm^3	FR4	2.4/3.5/5.9 GHz	2.3/2.6/3.7 dBi
[11]	Compact triple-band monopole antenna.	29 × 10 × 1.6 mm^3	FR4	2.45/3.45/5.5GHz	1.8/1.9/2.4 dBi
[12]	Square Loop CPW-Fed Printed Antenna	30 × 35 × 1.524 mm^3	Rogers 4350B	4.28 GHz, 6.68 GHz	1.05 dBi, 2.42 dBi
[13]	Compact Coplanar Waveguide-fed Planar Antenna	28 × 31 × 0.8 mm^3	FR4	3.7, 5.2 and 9.2 GHz	2.2−5.8 dBi
[14]	Penta-band Spiral Antenna for Vehicular Communications	18 × 18 × 0.254 mm^3	Rogers RT-5870	1.2 GHz	1.07 dBi
[15]	Tri-Band Hexagonal Microstrip Patch Antenna Using Modified Sierpinski Fractal	75 × 75 × 0.76 mm^3	Neltec NX9320	1.575 GHz, 5.9 GHz, 7.2 GHz	7.84 dBi, 7.96 dBi
[16]	Omnidirectional Low-Profile Multiband Antenna for Vehicular Telecommunication	70 mm × 80 mm × 6 mm	FR4	1.14, 1.91, and 2.45 GHz	> 1.7 dBi

Recent studies demonstrate that integrating Split Ring Resonators (SRRs) enhances antenna gain and bandwidth by manipulating electromagnetic properties. Recent works also highlight improved Multi-Input Multi-Output (MIMO) configurations and polarization control for robust vehicular links. Additionally, analytical investigations of 1D and 2D antenna arrays emphasize their suitability for mmWave vehicular systems, enabling better beamforming and diversity [17]. These advancements inform the design of the proposed tri-band coplanar decagon antenna with an octagonal SRR metasurface, addressing the needs of next-generation vehicular networks with improved size, gain, and efficiency [18, 19].

II. MATERIALS AND METHODS

The word "metamaterial," which has Greek roots, refers to something that deviates from typical natural qualities [20]. Enhancing efficiency and bandwidth sometimes requires sacrificing antenna size when building antennas out of naturally occurring materials. Conversely, incorporating a metasurface plane into the antenna design transforms and significantly increases efficiency. Reduced permittivity and permeability—usually linked to negative values for these parameters—are made possible by metasurfaces. This reduction makes it possible to raise frequency without expanding the physical dimension of the antenna. Hence, a wider bandwidth is achieved without typically increasing the antenna's size. The four concentric, decagon-shaped rings comprising the SRR construction each include gaps that are placed purposefully as shown in Fig. 1. Each ring is positioned with care so that it lines up with the arrangement of the spaces between with the adjacent ring. In response to external stimuli, such as a temporally fluctuating magnetic field aligned orthogonally to the resonator geometric plane, current is induced to flow through the rings. This generated current of solenoidal character gives the SRR structure the appearance of a resonant magnetic dipole. As a result, a dipolar distribution is seen in the magnetic-field pattern that emerges from the SRR [21]. Fig. 2 describes these negative properties of the metasurface antenna.

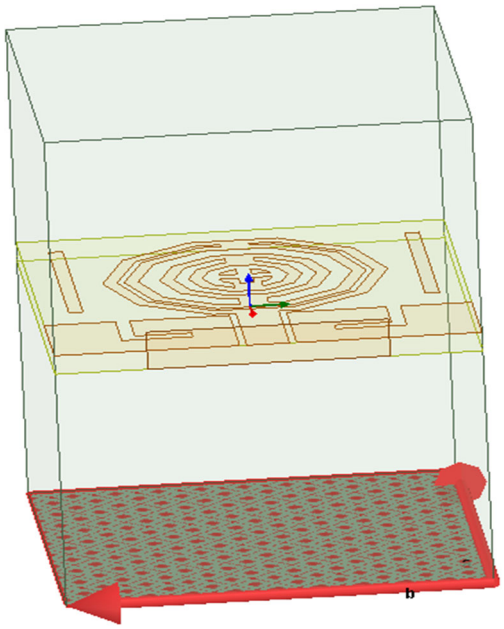

(a)

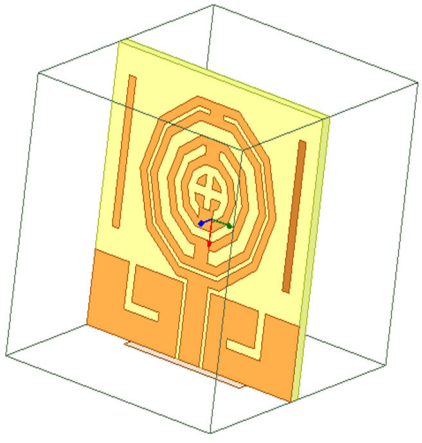

(b)

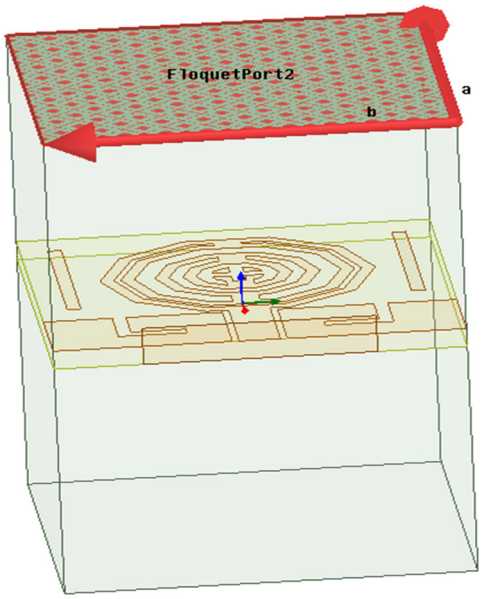

(c)

Fig. 1. SRR construction: (a). Setup for measurement of metamaterial characteristics, (b). Floquet port 1(Bottom), (c). Floquet port 2 (Top).

The mathematical analysis of the basic antenna design is given below [22]:

Calculation of Width (W):

$$W = \frac{C}{2fo\sqrt{\frac{(\varepsilon r+1)}{2}}}$$

Calculation of effective dielectric constant ($\in reff$):

$$\in reff = \frac{\varepsilon r+1}{2} + \frac{\varepsilon r-1}{2}\left[1 + 12\frac{h}{W}\right]^{-1/2}$$

Calculation of the Effective Length (L_{eff}):

$$L_{eff} = \frac{C}{2fo\sqrt{\epsilon reff}}$$

Calculation of the Length Extension (ΔL):

$$\Delta L = 0.412h\frac{(\varepsilon reff+0.3)(\frac{W}{h}+0.264)}{(\varepsilon reff-0.258)(\frac{W}{h}+0.8)}$$

Calculation of actual length of patch (L):

$$L = L_{eff} - 2\Delta L$$

Calculation of the ground plane dimensions (L_g and W_g):

$$L_g = 6h + 2L$$

$$W_g = 6h + 2W$$

The impedance of the patch can be given by:

$$z_a = 90\frac{\varepsilon_r^2}{\varepsilon_{r-1}}(\frac{L}{W})\text{^}2$$

The characteristic impedance of the transmission section can be given by:

$$Z_T = \sqrt{50 + Z_a}$$

The width of the transmission line can be given by:

$$Z_T = \frac{60}{\sqrt{\varepsilon_r}}\ln(\frac{8h}{W_T} + \frac{W_T}{4h});$$

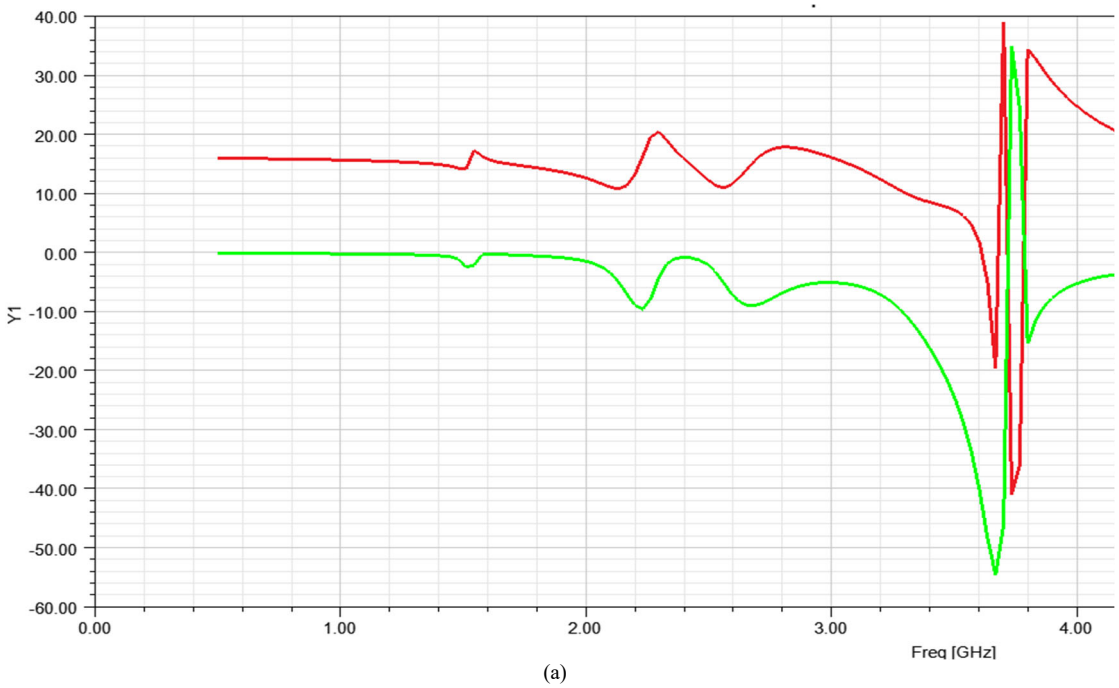

(a)

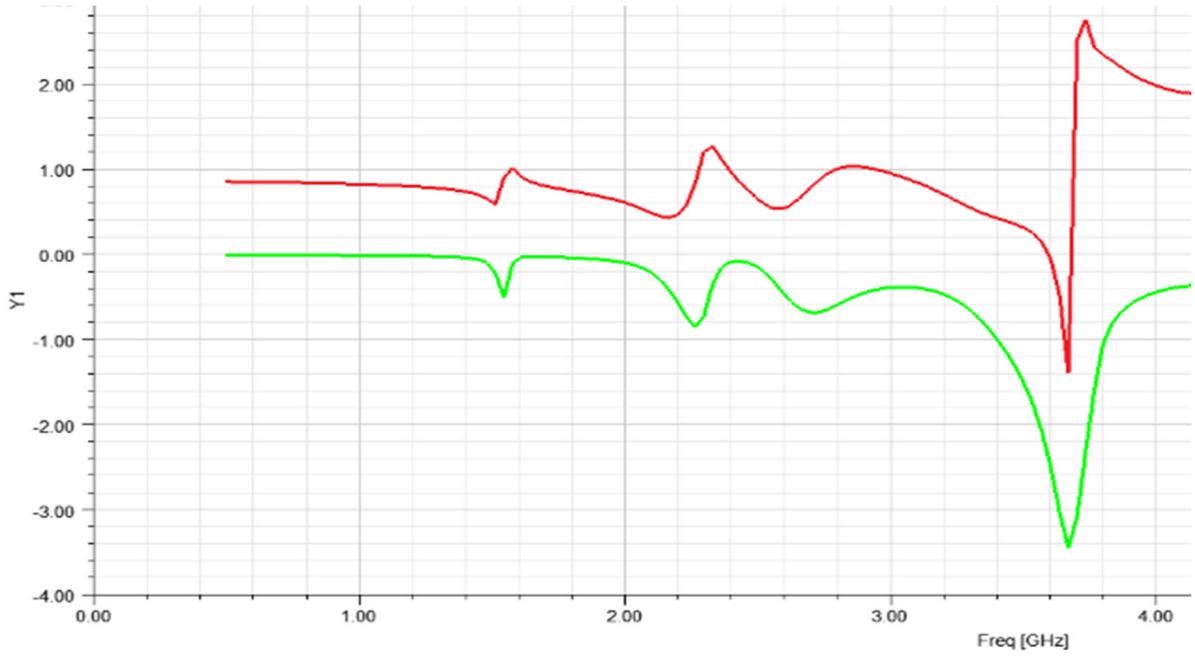

(b)

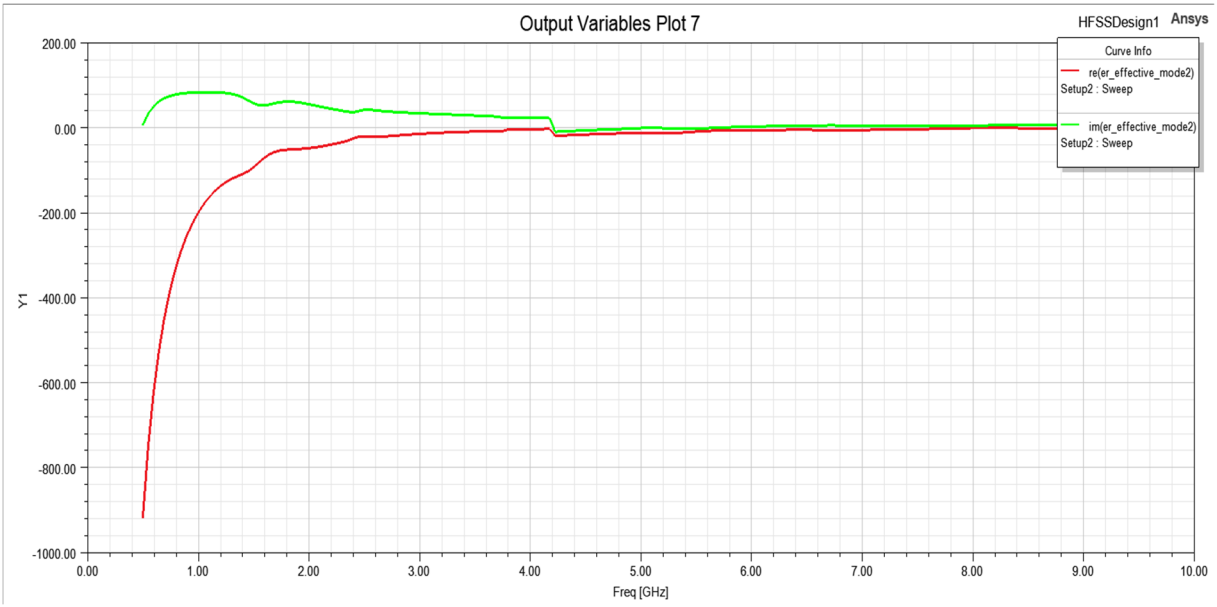

(c)

Fig. 2. Properties of the metasurface antenna: (a). Permeability v/s frequency plot, (b). Permittivity vs frequency plot, (c) Refractive index VS frequency.

III. Design of Proposed Antenna

The antenna configuration, depicted in Fig. 3(a), was carefully designed with FR4 (flame retardant) material, characterized by a dielectric constant of 4.4 and a loss tangent of 0.02. It was decided to use the widely accessible FR4 substrate, which has a height of 1.6 mm. This reduction in height enables an increase in frequency without the need for a larger size of the antenna. This in turn gives a wider bandwidth without the need for the usual antenna size increase. FR4 was selected as the substrate material for this antenna due to its widespread availability, affordability, and compatibility with standard PCB manufacturing processes. While FR4 does introduce higher dielectric losses and variability in dielectric constant potentially limiting the ultimate efficiency and frequency stability compared to low-loss substrates like Rogers or Taconic, it offers a robust balance of cost, mechanical strength, and fabrication ease, making it suitable for the high-volume, cost-sensitive requirements of automotive communications. Table II presents the proposed antenna's dimensional specifications.

TABLE II. Dimensional Specifications for the Antenna

Parameter	Ls	Ws	Lg	Wg	L1	L2	L3
Values (mm)	30	30	8	13	5	5	16
Paramete	S	R1	R2	R3	R4	R5	R6
Values (mm)	6.18	9	8.5	7.5	6	5	4
Parameter	R7	R8	R9	Wf	G	E	H
Values (mm)	3	2	1	0.5	1	4.4	1.6

The Split-Ring Resonator (SRR) is a novel addition to the monopole antenna design that allows us to attain the

necessary frequency spectrum for automotive applications. The antenna's performance is improved by this creative integration of SRR technology, guaranteeing excellent functioning in the context of vehicular communication networks. The decagon-shaped structure's resonance properties are a key factor in deciding how effectively the antenna operates. One of the primary factors affecting the resonant frequency indicated by '*f*' is the distance from the decagon's center to its vertex. The antenna is highly suited for automotive communication applications due to its deliberate placement and geometric configuration, which enhance its efficiency within the designated frequency range.

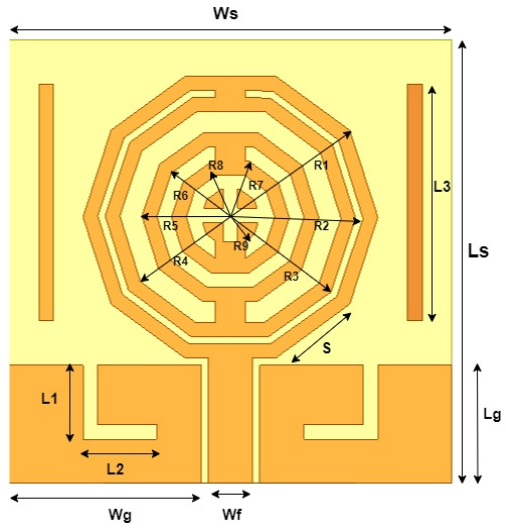

(a)

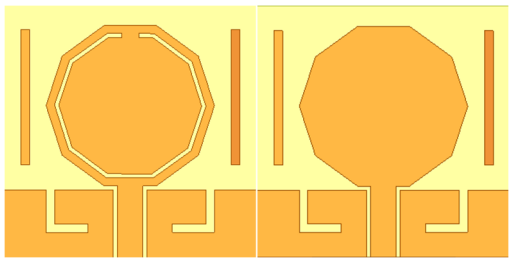

Stage-1 Stage-2

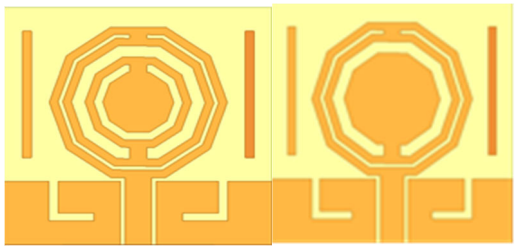

Stage-3 Stage-4

Stage-5

Stage-6

(b)

Fig. 3. Design of the antenna: (a). Geometry of the proposed antenna, (b). Design flow of the proposed antenna at various stages.

$$a = \frac{X_{mn}\, c}{2\pi f \sqrt{\varepsilon_r}} \tag{1}$$

where '*c*' indicates the speed of light, '*f*' resonant frequency, and 'X_{mn}' symbolizes the reactance of a circular monopole antenna in the TM11 mode, is set to 1.811. The side length 'S' of the decagon patch is determined by the below equation.

$$S^2 = \frac{2\pi a_e^2}{3\sqrt{3}} \tag{2}$$

where '*r*' represents the effective radius of the patch [15], and the value of S is calculated as 6.18 mm.

The steps involved in the implementation of the patch structure in the proposed antenna are the following:

- Using a conventional decagon, a patch with sides of size S=6.18mm is created in the first stage. There are two L-shaped holes in the ground and two parasitic components on either side of the patch.
- Taking inspiration from the monopole antenna, the second stage arrangement consists of the first ring of the Split Ring Resonator (SRR) with R1 = 9 mm and R2 = 8.5 mm.
- In the third stage, the initial ring is joined by a second ring that draws inspiration from the antenna. The measurements of this second ring are R3 = 7.5 mm and R4 = 6.0 mm.
- The Split Ring Resonator (SRR) third ring is constructed in the fourth stage, with dimensions R5 = 5.0 mm and R6 = 4.0 mm.
- Using R7 = 3.0 mm and R8 = 2.0 mm, the final ring is created in the last stage, Stage 5. The two-millimeter split gap is a feature that is present in every ring and is placed on opposite sides of the rings in a deliberate manner. In the last stage, known as Stage 6, as shown in Fig. 3(b), two rectangular holes are carved out of the construction of a normal decagon with a radius of R9 = 1 mm.

Full-wave electromagnetic simulations were performed using ANSYS HFSS (2019 R2 version). The simulation setup included precise geometry modeling of the antenna, material property definitions for FR4, and appropriate boundary conditions mimicking free-space radiation. Excitation was provided via a coaxial feed. Key performance parameters such as reflection coefficient

(S11), gain, radiation patterns, surface current distribution, radiation efficiency, Envelope Correlation Coefficient (ECC), and diversity gain were systematically evaluated. An iterative design approach with six stages was employed to refine the antenna configuration for optimal multi-band operation covering GPS, LTE, and Wi-Fi frequencies.

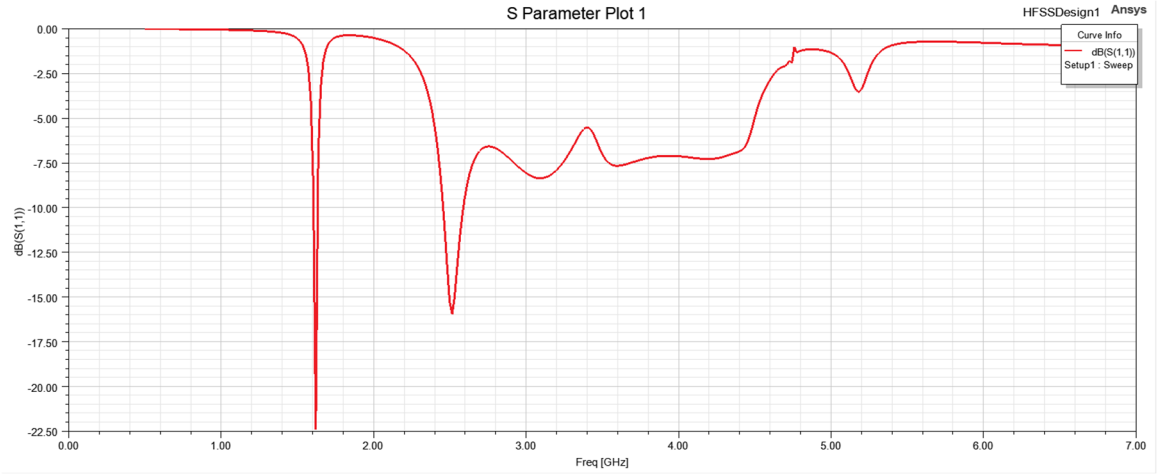

Stage-1

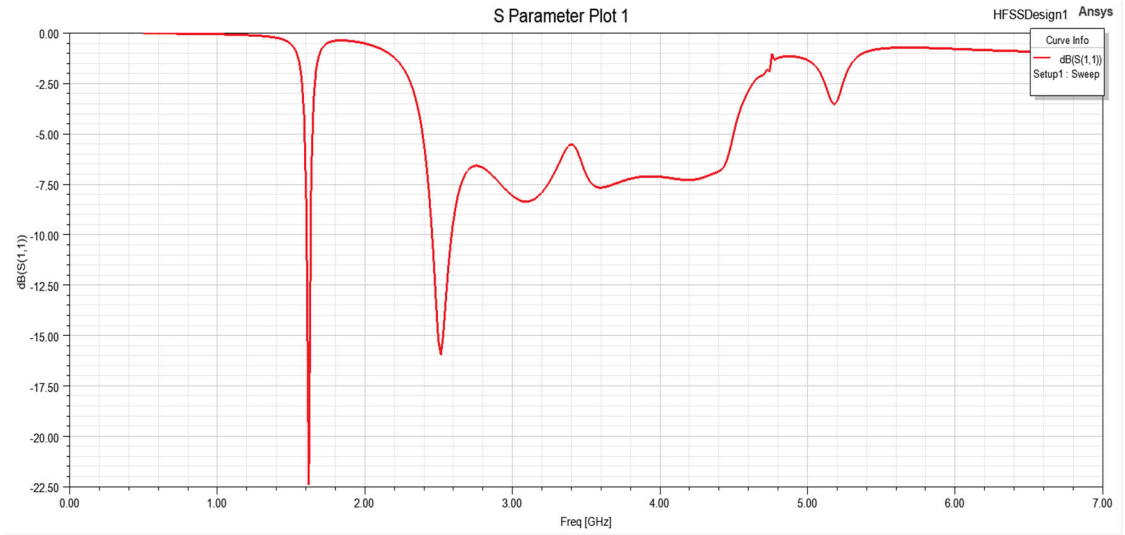

Stage-2

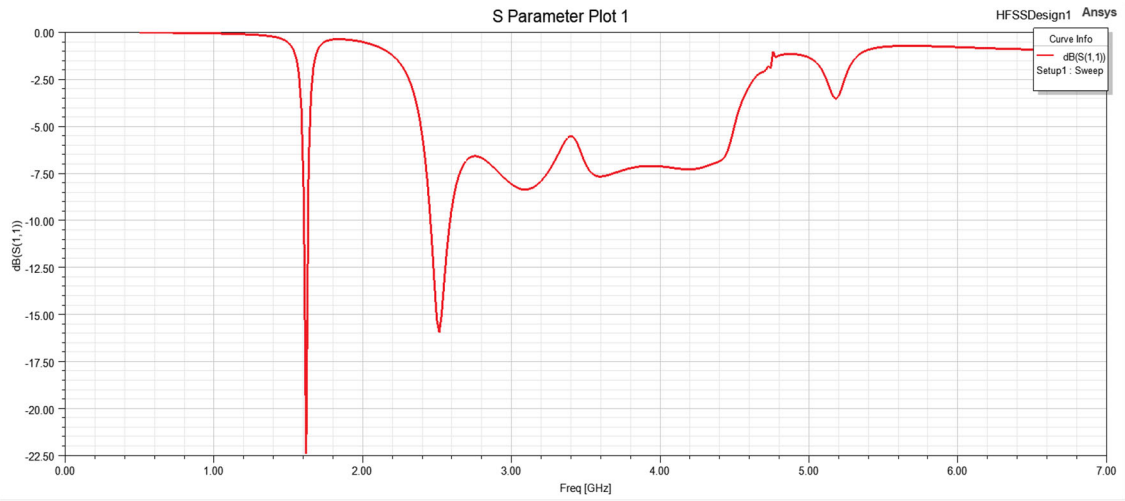

Stage-3

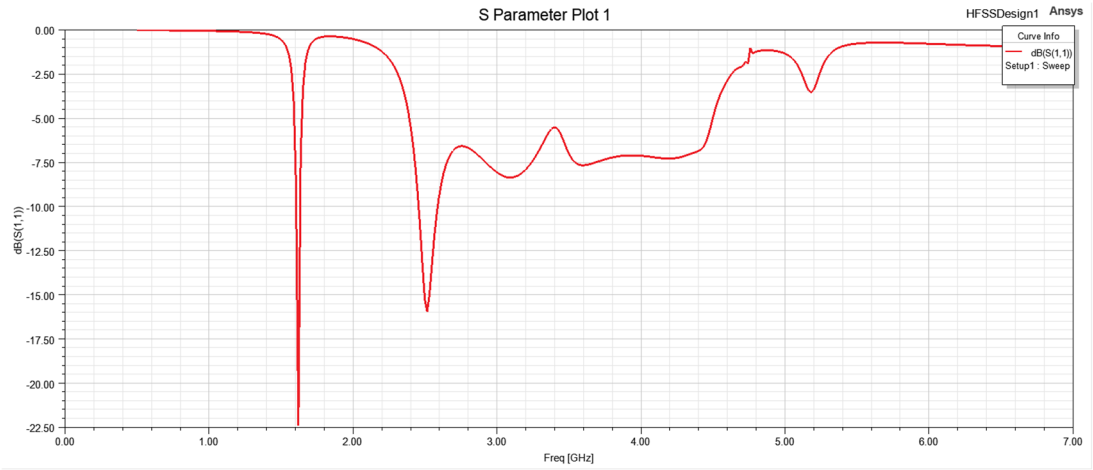

Stage-4

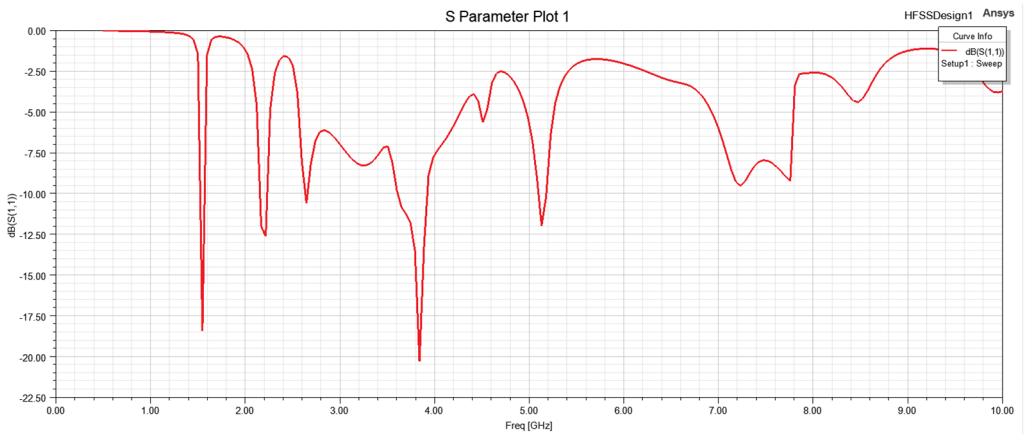

Stage-5

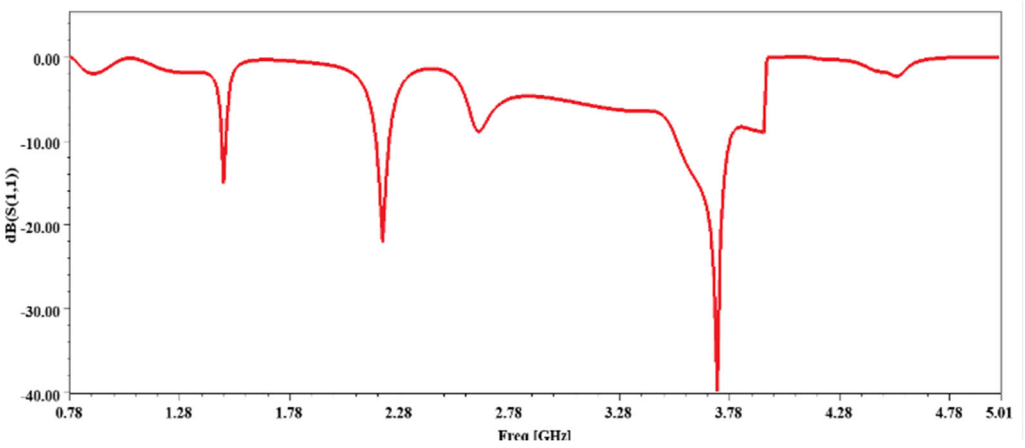

Stage-6

Fig. 4. Return loss vs Freq. plots of different Iterations from stage-1 to stage-6.

IV. Results and Discussions

A. Reflection Coefficient of the Proposed Antenna

The reflection coefficient, which is a critical parameter in antenna assessment, is analyzed by employing an iterative design method as shown in Fig. 4. The proposed antenna's initial iteration features are a central 2.4 GHz resonance frequency and a significant bandwidth of 100MHz. The antenna produces even more improvement in the second iteration by achieving an enhanced bandwidth of 110 MHz at a resonant frequency of 2.3 GHz.

The design exhibits remarkable dual-band behavior at the third iteration with frequencies of 1.6 GHz and 2.3 GHz of resonance. The fourth and fifth rounds of the iterative refining process take an interesting turn when a circular-shape etched patch using the Kotch fractal is inserted. This new adjustment leads to a significant bandwidth gain and the appearance of a multiband phenomenon. Resonating frequencies of 1.7 GHz, 2.3 GHz,

and 3.87 GHz are now shown by the antenna, demonstrating the effectiveness of the iterative design process and the special roles played by the Kotch fractal in determining the antennas performance characteristics.

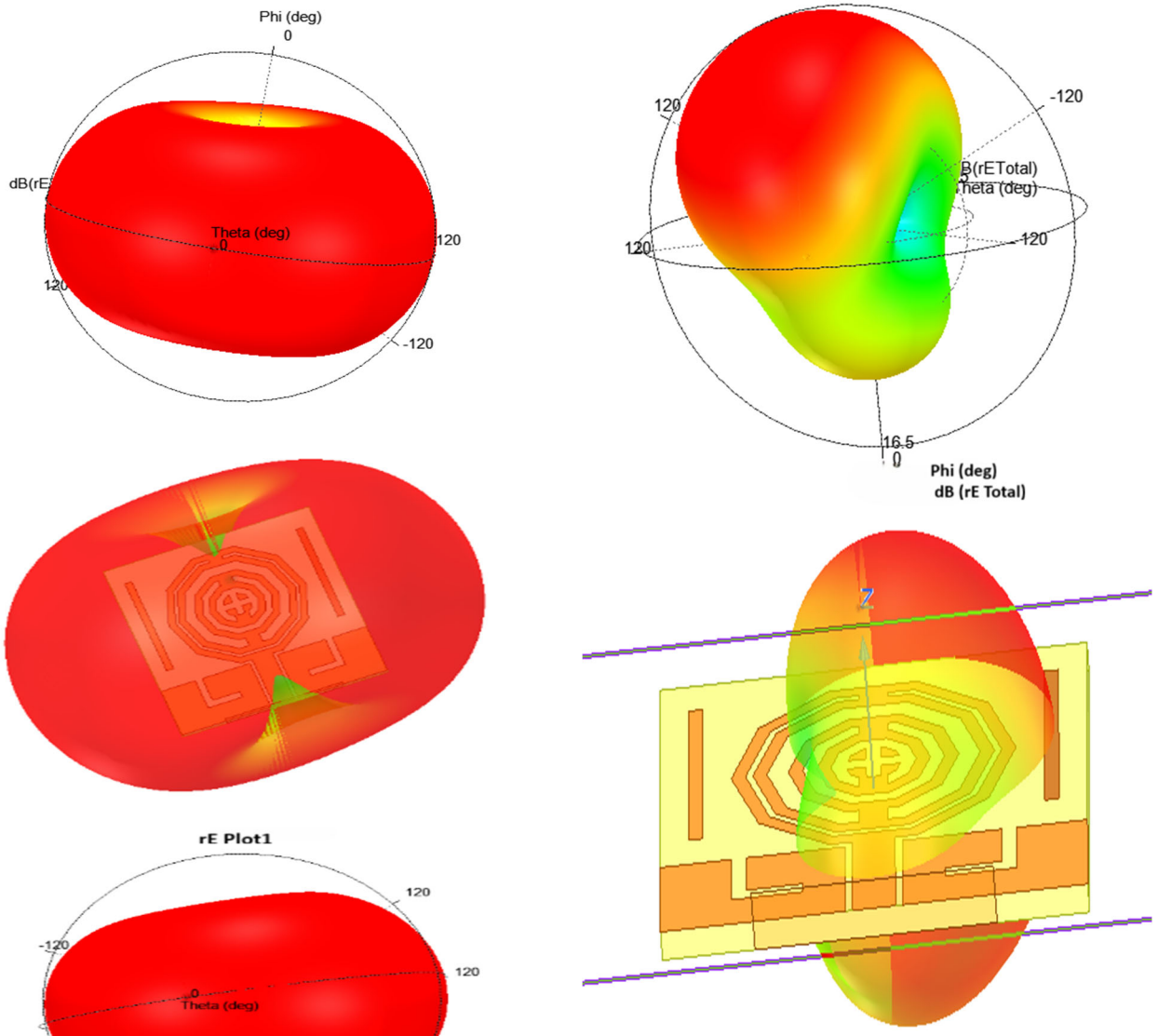

Fig. 5. Gain of the proposed antenna at 1.5 GHz, 2.2 GHz and 3.8 GHz.

B. Gain of the Proposed Antenna

Fig. 5 depicts the detailed examination of the Gain characteristics for the suggested antenna. Fig 5(a) illustrates the gain at 1.5 GHz, Fig 5(b) describes the gain at 2.2 GHz, and Fig. 5(c) describes the gain performance at 3.8GHz. Especially there is a considerable improvement in the antenna's gain from its initial measurement of 2 dBi to a high of 4.6 dBi. This enhancement highlights the effectiveness of the suggested antenna in a variety of frequency bands, highlighting its adaptability and enhanced performance.

C. Radiation Pattern

An antenna's electromagnetic energy distribution in space is described by its radiation pattern. The emission patterns at 1.5 GHz, 2.2 GHz, and 3.8 GHz of the suggested antenna. it describes how the device transmits

and receives electromagnetic waves at these particular frequencies as depicted in Fig. 6.

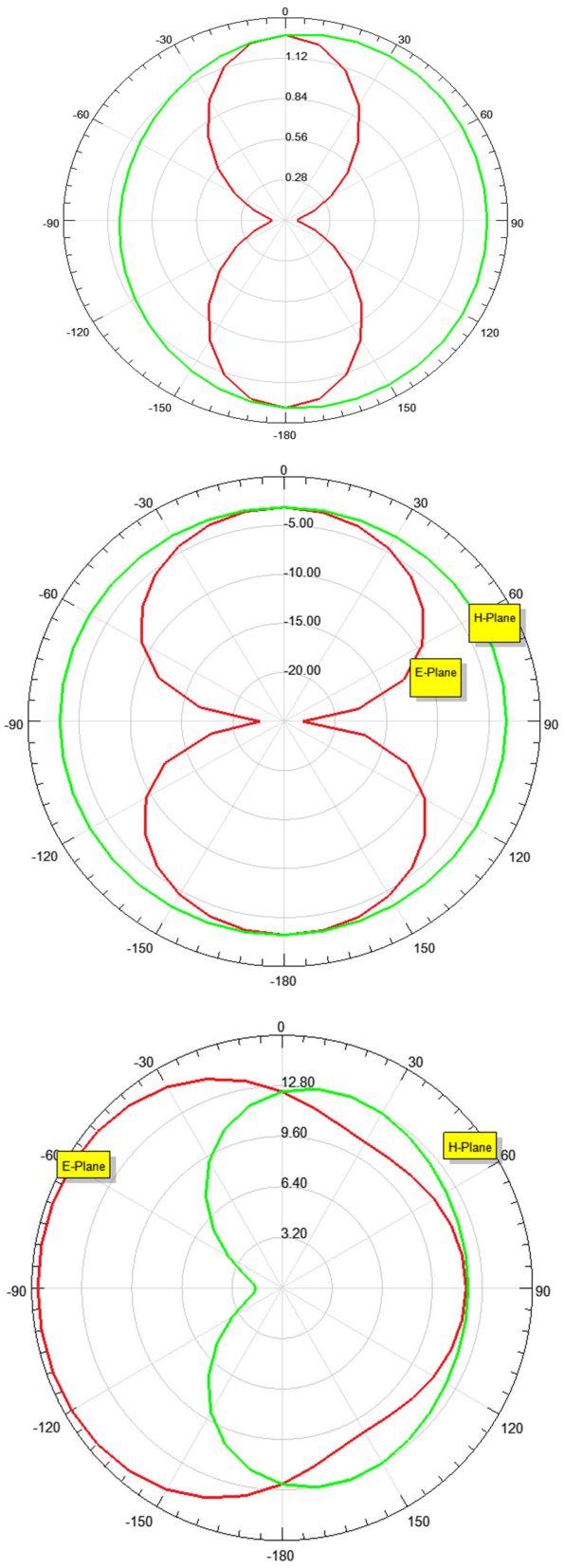

Fig. 6. Radiation pattern of the proposed antenna at 1.5 GHz, 2.2 GHz and 3.8 GHz.

The radiation pattern of the proposed antenna illustrates the geographical distribution of energy radiated at 1.5 GHz frequency. This pattern proves the coverage and directivity of the antenna propagates electromagnetic waves in all directions.

The radiation pattern changes when changes are made to 2.2 GHz to correspond with the antenna's characteristics at this higher frequency. Changes in the pattern indicate adjustments made to the antenna's beam width, side lobes, and radiation efficiency overall.

The radiation pattern further adjusts to the unique properties of this frequency at 3.8 GHz. Understanding the pattern at this frequency is essential to evaluate the antenna's performance at high-frequency applications, since several design factors such as height, length and width of the antenna are involved.

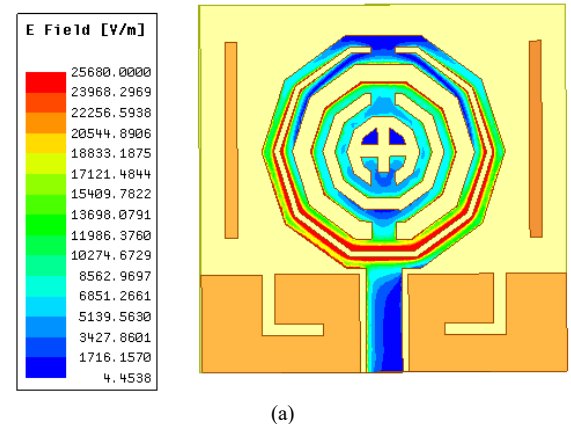

(a)

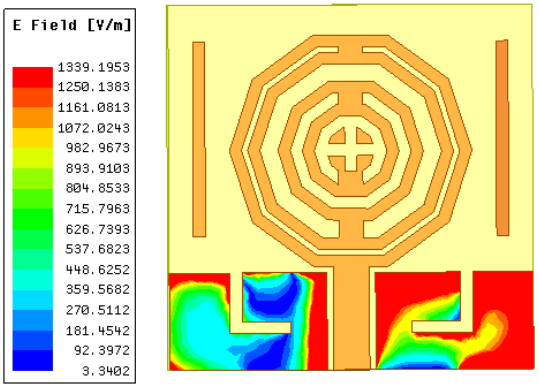

(b)

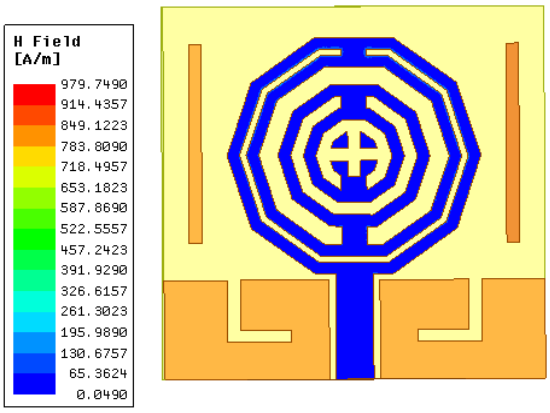

(c)

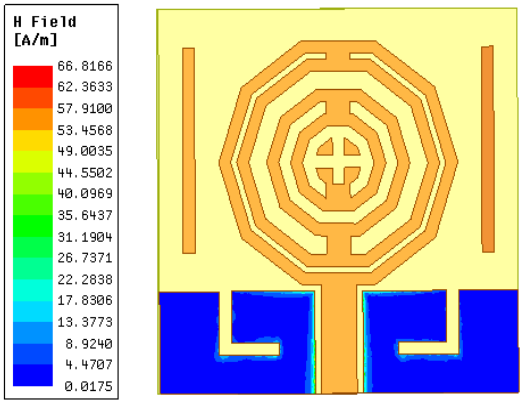

(d)

Fig. 7. represents the E-field and H-field of the proposed antenna: (a). E Field of the main patch, (b). E Field of the ground and parasitic elemets, (c). H Field of the main patch, (d). H Field of the ground.

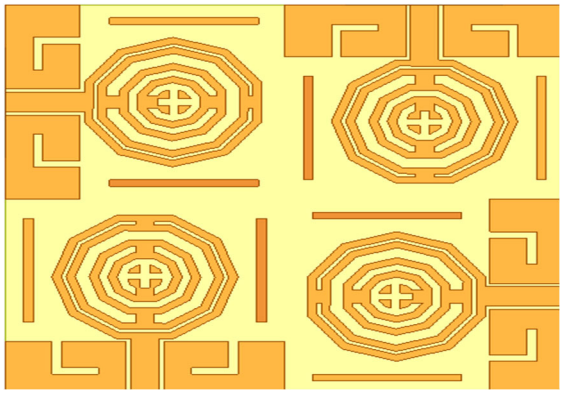

Fig. 8. Geometrical view of the proposed antenna.

D. Current Distribution

Fig. 7 gives the current distribution of the single patch antenna. As seen in Fig. 8, this low-loss characteristic is maintained for every port, confirming the antenna's reliable operation. In addition, the antenna has a remarkable bandwidth of 500MHz in three different frequency bands, which enhances its adaptability and efficiency in a variety of operational situations. The S-parameter plot of the antenna is depicted in Fig. 9, providing important details about its performance attributes. The suggested antenna is noteworthy for having a very low reflection coefficient; it reaches −30 dB which indicates very little signal loss.

The antenna is carefully crafted from FR4 (flame retardant) material by choosing a dielectric constant of 4.4 with a loss tangent of 0.02 for maximum performance as shown in the Fig. 10. Measuring 60 × 60 × 1.6 mm, its proportions serve a variety of purposes, including LTE, Wi-Fi, INSAT, GPS (global positioning system), and vehicular communication. Across a range of communication and navigation systems, this thoughtful design guarantees adaptability and efficiency.

E. Envelope Correlation Coefficient (ECC)

The envelope correlation coefficient of 0.01 is measured during testing to assess amplitude changes across the four ports of the proposed antenna, which is shown in Fig. 11. This indicates that there are no connections between the amplitude fluctuations at each port of the antenna, indicating effective spatial diversity and pointing to the possibility of better MIMO system performance.

F. Diversity Gain

The relationship between a MIMO antenna system's diversity gain and its envelope correlation coefficient (ECC) value is often inverse. According to the observations from Fig. 12, the suggested MIMO antenna has a notable diversity gain of 10. This demonstrates how using several channels or pathways inside the antenna system may effectively increase reliability and performance, especially in demanding communication scenarios.

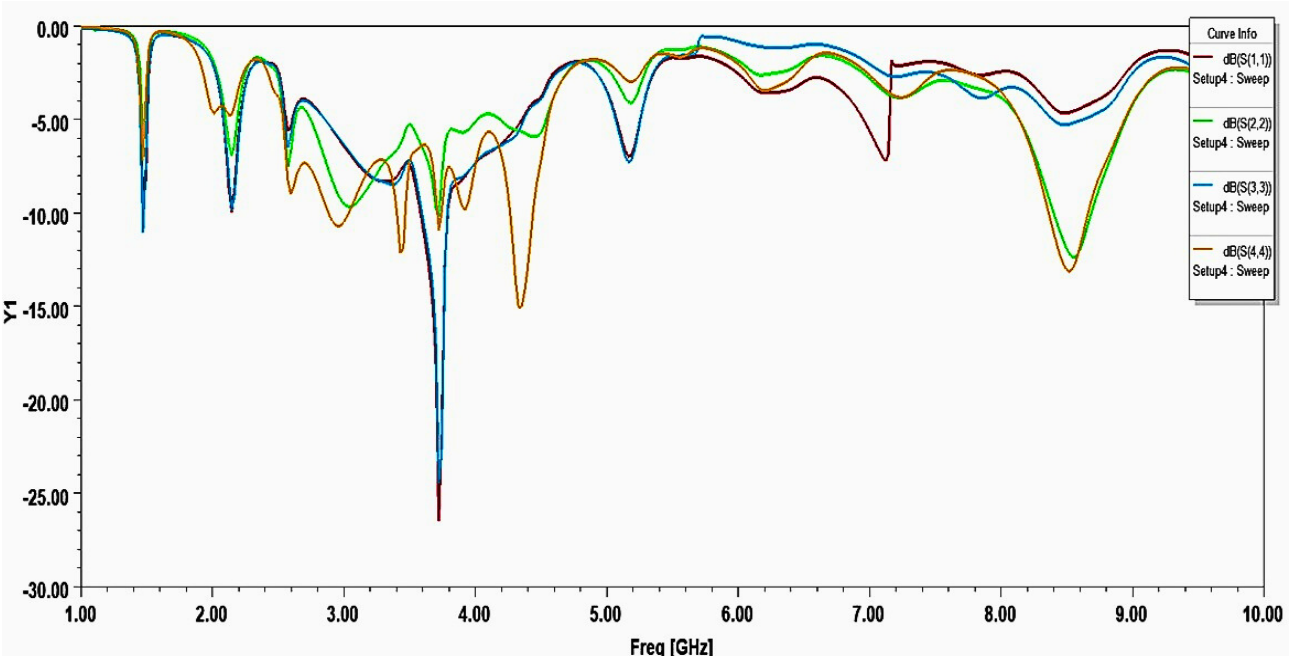

Fig. 9. The S-parameter of the proposed antenna.

G. Antenna Installed on the Car's Roof

The suggested antenna is positioned on the car's roof in a manner that, as depicted in Fig. 13, results in an electrical size significantly larger than the antenna's physical dimensions. The analysis also takes into account situations in which the antenna is fixed to the vehicle's front bumper. The simulations to assess the antenna's performance in different locations are meticulously conducted using the ANSYS HFSS 2019 R2 version.

Fig. 10. Fabricated model of the designed antenna (Top & Bottom).

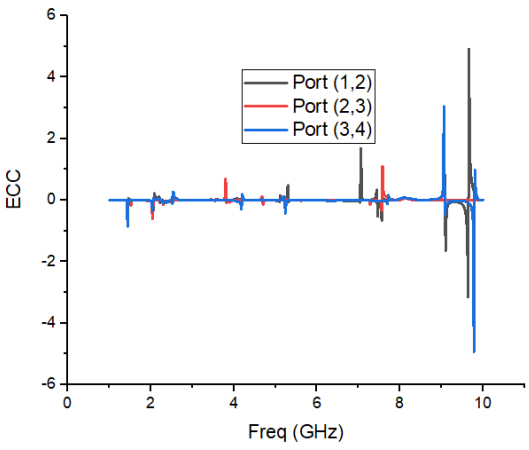

Fig. 11. ECC value of the proposed antenna.

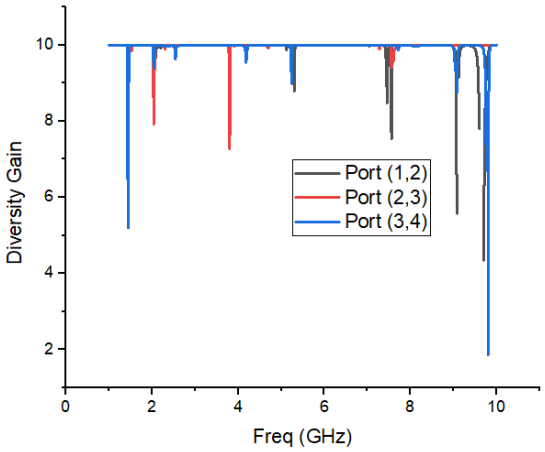

Fig. 12. Diversity gains plot of the proposed antenna.

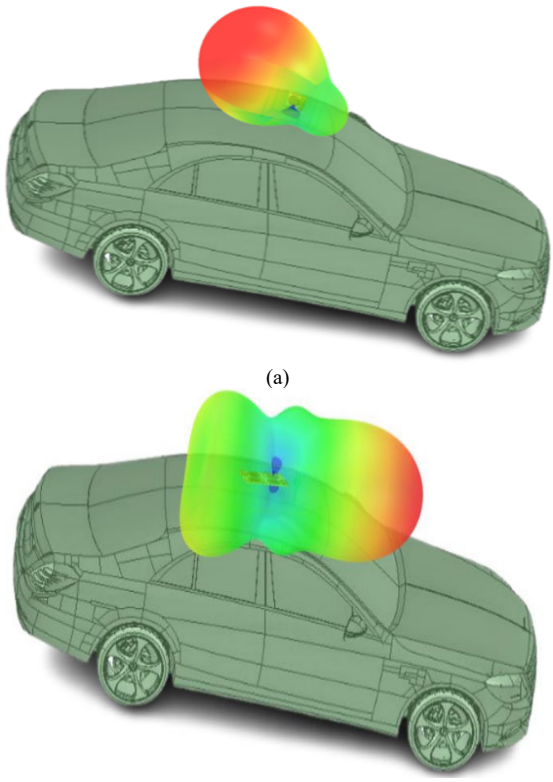

(a)

(b)

Fig. 13. Antenna installed on the roof of the car: (a). Using a single element, (b) Using a MIMO arrangement.

H. Comparison of Simulated Proposed with Existing different Antennas

Table III presents a comparative analysis between the proposed antenna at different stages. Table IV presents a comparative analysis between the proposed antenna and existing works. After mounting the suggested antenna on the vehicle's roof, the measured gain was 4.6 dBi. In addition, the antenna's remarkable 80% radiation efficiency was noted, confirming its efficiency once it was mounted on the car's roof (see Fig. 14).

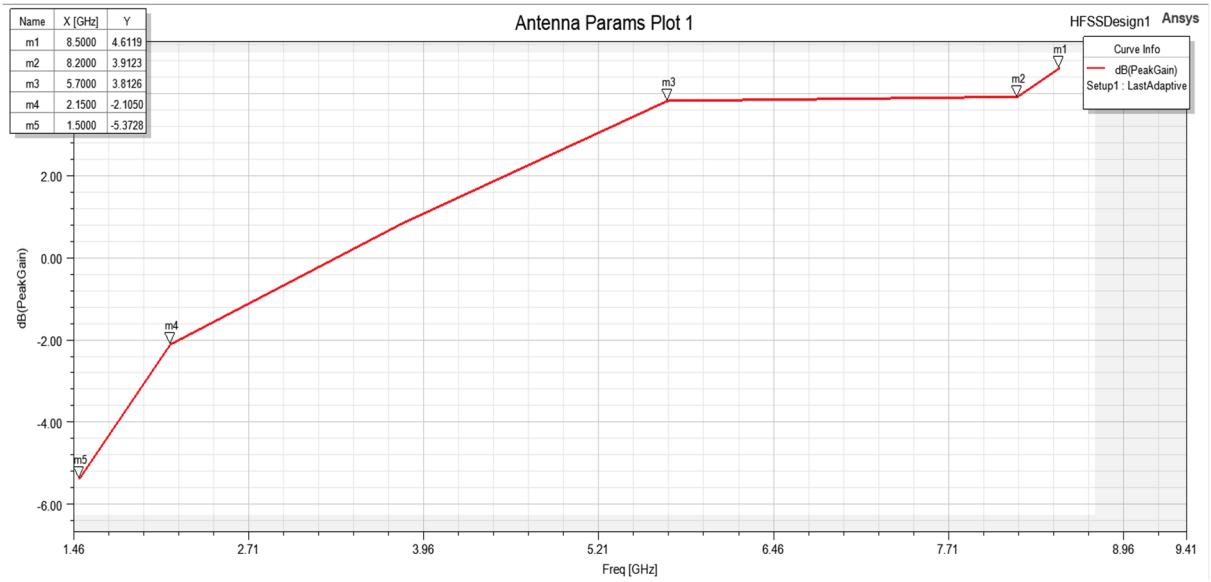

Fig. 14. Measured gain of MIMO antenna against frequency.

TABLE III. COMPARISON OF THE PROPOSED ANTENNA AT DIFFERENT STAGES

Parameter Iteration wise	S11 (dB)	VSWR	Bandwidth (MHz)	Gain (dB)	Efficiency (%)
Stage-1	−18	1.07	100	3.2	60
Stage-2	−23	1.08	110	1.1	70.2
Stage-3	−24	1.05	50, 120	2.2,1.1	72
Stage-4	−25	1.1	100, 110, 200	3,1.1,2.2	73
Stage-5	−23	1.2	100, 110, 200	3.2,1.1,2,2	75
Stage-6	−35	1.1	100, 110, 500	3.2, 1.13, 4.6	87

TABLE IV. COMPARISON OF PROPOSED ANTENNA WITH OTHER ANTENNAS

Ref No.	Patch	Dimensions	Substrate Material	Operating Frequency	Gain	Efficiency
[23]	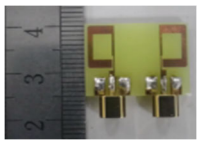	15.5 × 18 x 1.6 mm^3	FR4	2.41 GHz	0.72 dBi	78%
[24]	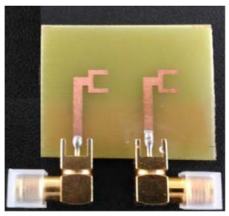	26 x 34 x 0.8 mm^3	FR4	2.5-10.7 GHz	4.3 dBi	80%
[25]	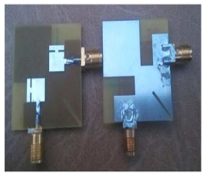	28 × 31 × 0.8 mm^3	FR4	4.7–10 GHz	1.7-4.2 dBi	60%
[26]	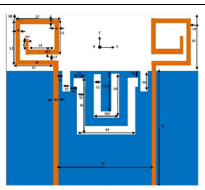	70 × 70 × 0.8mm^3	FR4	1.2 GHz	2.5 dBi	-

[27]	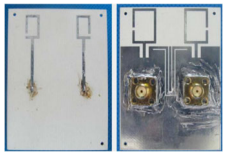	**50 × 17 × 0.8 mm³**	**CEM-1 S3110**	**1.5, 2, 2.5, 5 & 7 GHz**	**2 dBi**	**70%**
Proposed work	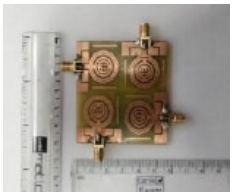	**60 × 60 × 1.6 mm³**	**FR4**	**1.5/ 2.6/3.7/4/ 7.2/8.2/8.7 GHz**	**4.6 dBi**	**87%**

V. Conclusion

The proposed antenna design constitutes a triple-band decagon-shaped antenna suitable for applications such as GPS (Global Positioning System), LTE, Wi-Fi, and vehicle communication. The antenna is built on a 30 × 30 × 1.6 mm³ FR-4 substrate and has resonance frequencies of 1.5 GHz, 2.2 GHz, and 3.8 GHz. Comparable respective maximum gains are −3.2 dB, 1.13 dB, and 3 dB, in that order. The antenna achieves simulated radiation efficiencies ranging from 60% in baseline designs to 75% after incorporating the metasurface structure, while measured efficiencies of the MIMO antenna mounted on a vehicle roof reach 87%. Likewise, the peak gain of 4.6 dBi reported corresponds to the measured value obtained after prototype fabrication and vehicle mounting, demonstrating a significant improvement over initial simulated gain of approximately 2 dBi. Notably, at 2.2 GHz, a maximum radiation efficiency of 75% is attained. Moreover, the suggested MIMO antenna design exhibits resonance across a wide frequency ranging from 1.5 GHz to 8.7 GHz and achieves a remarkable peak gain of 4.6 dBi and an exceptional radiation efficiency of 87%. These simulations included the examination of scattering parameters, 2D/3D radiation pattern plots, and surface current distribution. To confirm the simulation results, practical return loss characteristics were tested under appropriate conditions

Conflicts of Interest:

The authors declare no conflict of interest.

Author Contributions

Akansha Gupta and Purnima K Sharma were primarily responsible for drafting the main manuscript text, conducting literature research, methodology, and organizing the content; T. J. V. Subrahmanyeswara Rao and T. V. N. L. Aswini were actively involved in the practical aspects of the research, specifically in antenna fabrication and testing; Dinesh Sharma contributed to the review process by providing valuable insights and recommendations; all authors had approved the final version.

References

[1] M. F. Tufvesson, J. Karedal, and C. Mecklenbräuker, "A survey on vehicle-to-vehicle propagation channels," *IEEE Wireless Commun*., vol. 16, no. 6, pp. 12–22, 2009.

[2] S. Arumugam, S. Manoharan, S. K. Palaniswamy, and S. Kumar, "Design and performance analysis of a compact quad-element UWB MIMO antenna for automotive communications," *Electronics*, vol. 10, 2021.

[3] V. Saritha and C. Chandrasekhar, "A conformal multi-band MIMO antenna for vehicular communications," *Progress in Electromagnetics Research Letters*, vol. 108, pp. 49–57, 2023.

[4] M. Kanagasabai, S. Shanmuganathan, M. G. N. Alsath, and S. K. Palaniswamy, "A novel low-profile 5G MIMO antenna for vehicular communication," *International Journal of Antennas and Propagation*, October 2022.

[5] B. T. Madhav, T. Anilkumar, and S. K. Kotamraju, "Transparent and conformal wheelshaped fractal antenna for vehicular communication applications," *AEU-International Journal of Electronics and Communications*, vol. 91, pp. 1–10, Jul. 1, 2018.

[6] D. S. Woo, "A triple band C-shape monopole antenna for vehicle communication application," *Progress in Electromagnetics Research C*, vol. 121, pp. 97–106, 2022.

[7] M. P. Joshi and V. J. Gond, "Design and analysis of microstrip patch antenna for WLAN and vehicular communication," *Progress in Electromagnetics Research C*, vol. 97, pp. 163–176, 2019.

[8] C. T. P. Song, P. S. Hall, and H. G. Shiraz, "Multiband multiple ring monopole antennas," *IEEE Transactions on Antennas and Propagation*, vol. 51, no. 4, April 2003.

[9] P. Iyampalam and I. Ganesan, "Meta-material inspired penta-band decagon fractal antenna for wireless applications, e-Prime," *Advances in Electrical Engineering, Electronics and Energy*, vol. 6, 2023.

[10] K. Patchala, Y. R. Rao and A. M. Prasad, "Triple band notch compact MIMO antenna with defected ground structure and split ring resonator for wideband applications," *Heliyon*, vol. 6, 2020.

[11] Y. Zheng, P. Wang, M. Hua, and P. Gao, "Compact triple-band monopole antenna for WLAN/WiMAX applications," *IEICE Electron. Express*, vol. 10, 2013.

[12] P. C. Ooi and K. T. Selvan, "The effect of ground plane on the performance of a square loop CPW-Fed printed antenna," *Prog. Electromagnetics Research Letters*, vol. 19, pp. 103–111, 2010.

[13] A. Subbarao and S. Raghavan, "Compact coplanar waveguide-fed planar antenna for ultra-wideband and WLAN applications," *Wireless Pers Commun*, vol 71, pp. 2849–2862, 2013.

[14] R. T. R. Rao, "Design and performance analysis of a penta-band spiral antenna for vehicular communications," *Wireless Pers Commun*, vol 96, pp. 3421–3434, 2017.

[15] T. Mondal, S. Samanta, R. Ghatak, and S. R. B. Chaudhuri, "A novel tri-band hexagonal microstrip patch antenna using modified sierpinski fractal for vehicular communication," *Progress in Electromagnetics Research C*, vol 57, pp. 25–34, 2015.

[16] W. Lee, Y. K. Hong, J. J. Lee, J. H. Park, and W. Seong, "Omnidirectional low-profile multiband antenna for vehicular telecommunication," *Progress in Electromagnetics Research Letters*, vol. 51, pp. 53–59, 2015.

[17] M. Q. Abdalrazak, A. H. Majeed, and R. A. A. Alhameed, "An analytical investigation on the performance of 1D and 2D antenna arrays for MM-Wave modern communication systems," *Iraqi Journal of Information & Communications Technology*, vol 6, no. 2, pp. 78–88, 2023.

[18] P. K. Sharma, D. Sharma, T. J. V. S. Rao, J. R. Szymański, M. Ż. Mortka, and M. Sathiyanarayanan, "Design and implementation of a meta-material based ultra-wide band microstrip patch antenna for vehicular communication," *Microsystem Technologies*, 2024

[19] P. K. Sharma, J. R. Szymański, M. Ż. Mortka, M. Sathiyanarayanan, and D. Sharma, "Design and analysis of four-leaf clover shaped MIMO antenna for Sub-6 GHz V2X applications," *Frequenz*, vol. 78, pp. 347–362, 2024.

[20] S. Rajasri and R. B. Rani, "Design and performance analysis of metamaterial-inspired decagon-shaped antenna for vehicular communications," *Progress in Electromagnetics Research Letters*, vol. 105, pp. 139–147, 2022.

[21] I. Bulu, H. Caglayan, K. Aydin, and E. Ozbay, "Compact size highly directive antennas based on the SRR metamaterial medium," *New Journal of Physics*, vol 7, 2005.

[22] H. M. Marhoon, H. A. Abdulnabi, and Y. Y. A. Aboosi, "Designing and analysing of a modified rectangular microstrip patch antenna for microwave applications," *Journal of Communications*, vol. 17, no. 8, pp. 668–674, 2022.

[23] L. S. Yang, T. Li, and S. Yan, "Highly compact MIMO antenna system for LTE/ISM applications," *International Journal of Antennas and Propagation*, 2015.

[24] J. C. Rao and N. Venkateswara Rao, "Compact UWB MIMO slot antenna with defected ground structure," *ARPN J. Eng. Appl. Sci*., vol. 11, no. 17, 2016.

[25] J. Ren *et al*., "Compact printed MIMO antenna for UWB applications," *IEEE Antennas and Wireless Propagation Letters*, vol. 13, 2014.

[26] F. Ahmed, H. M. Chowdhury, and A. A. Rahman, "A multiband MIMO antenna for future generation handset applications," in *Proc. International Conference on Electrical, Computer and Communication Engineering (ECCE)*, 2017, pp. 16−18, 2017.

[27] X. Zhou, X. L. Quan, and R. L. Li, "A dual-broadband MIMO antenna system for GSM/UMTS/LTE and WLAN handsets," *IEEE Antennas and Wireless Propagation Letters*, vol. 11, 2012.